

Detection Range of Intercept Sonar for CWFM Signals

Jacek MARSZAL, Roman SALAMON

*Department of Marine Electronic Systems
Faculty of Electronics, Telecommunications and Informatics
Gdansk University of Technology*

Narutowicza 11/12, 80-233 Gdańsk, Poland; e-mail: jacek.marszal@eti.pg.gda.pl

(received February 3, 2014; accepted May 5, 2014)

Stealth in military sonars applications may be ensured through the use of low power signals making them difficult to intercept by the enemy. In recent years, silent sonar design has been investigated by the Department of Marine Electronic Systems of the Gdansk University of Technology. This article provides an analysis of how an intercept sonar operated by the enemy can detect silent sonar signals. To that end a theoretical intercept sonar model was developed with formulas that can numerically determine the intercept ranges of silent sonar sounding signals. This was tested for a variety of applications and water salinities. Because they are also presented in charts, the results can be used to compare the intercept ranges of silent sonar and traditional pulse sonar.

Keywords: intercept sonar, silent sonar, CWFM signal, detection, detection range.

1. Introduction

Sonars and echo sounders emit sounding signals which may be detected by intercept passive sonar on board military ships (BOYD *et al.*, 1961; FRIEDMAN, 2006; THALES-SAFARE, 2012), as well as shipping noise (GRELOWSKA *et al.*, 2013; KOZACZKA, GRELOWSKA, 2004; KOZACZKA *et al.*, 2007; KOZACZKA, GRELOWSKA, 2011). Once detected, sounding signals give away the potential presence of an enemy ship in the area under surveillance which is an obvious risk to the sonar's carrier. To reduce this risk sounding signals must be made more difficult to detect. This can be achieved by using less powerful signals and wide spectrum continuous signals (FULLER, 1990; SKOLNIK, 2008). If equipped with these features, the sonar is called silent sonar or low probability of intercept sonar (LPI sonar) (MARSZAL, SALAMON, 2012; 2013; SALAMON *et al.*, 2011; WILLETT *et al.*, 2004).

The basic criterion that a silent sonar design must meet is that its operation will be comparable to that of its classic counterpart. Analyses and simulation tests have shown that this is possible with a significantly reduced sounding signal power (MARSZAL, 2014; MARSZAL, SALAMON, 2013; SALAMON, MARSZAL, 2013). As a result, the sounding signal detection distance will certainly be shorter for intercept sonar.

The distance over which intercept sonars can detect sounding signals depends not only on their power but also on their parameters (i.e. shape of autocorrelation function, directivity pattern and so on) and acoustic wave propagation in the body of water (SALAMON, MARSZAL, 2013; MARSZAL, 1992).

In the article we will present the results of theoretical analysis and simulation tests of how the parameters of silent sonar sounding signals impact intercept sonar detection and, by the same token, the intercept distance. To that end we are going to use a model of intercept sonar using envelope detection, energy detection and energy spectral density analysis. While they are known methods of detection, we will study them for how they can receive an untypical continuous signal emitted by silent sonar. We will leave out Doppler effect on silent sonar operation (MARSZAL, 2014; MARSZAL, SALAMON, 2012), due to its insignificance for intercept sonar sounding signal detection.

2. General description of the problem

Sonar range estimation is commonly conducted by solving the range equation in logarithmic form (HODGES, 2010; SALAMON, 2006; URICK, 1996). It was also used for the intercept sonar under the assumption that it detects typical sounding pulses of sonar

(THALES-SAFARE, 2012; WAITE, 2002). By using range equations, we are going to show which parameters of silent sonar and intercept sonar are decisive for the relation between the ranges of both sonars.

The compact form of the sonar range equation can be written as:

$$SNR = EL - NL \quad [\text{dB}], \quad (1)$$

where SNR is the minimal input signal-to-noise ratio which ensures that the detection conditions are as assumed with detection occurring at receiver input EL – the level of the acoustic signal received (i.e. the echo signal in the case of active sonar), and NL – ambient noise level.

The EL level is described with the formula:

$$EL = 20 \log \frac{p_s}{\sqrt{2} p_1}, \quad (2)$$

where p_s is the amplitude of acoustic pressure of a wave perpendicularly incident on the surface of sonar receiving transducer and $p_1 = 1 \mu\text{Pa}$ is the RMS value of the reference pressure.

The NL noise level can be expressed as:

$$\begin{aligned} NL &= 10 \log \frac{\sigma^2}{p_1^2} = 10 \log \frac{N_1 B}{p_1^2} \\ &= 10 \log \frac{N_1}{p_1^2 / B_1} + 10 \log \frac{B}{B_1}, \end{aligned} \quad (3)$$

where σ^2 is the variance of noise acoustic pressure on the receiving transducer surface measured in the receiver bandwidth B , while N_1 is the spectral density of noise intensity, and $B_1 = 1 \text{ Hz}$.

The expression:

$$SPL = 10 \log \frac{N_1}{p_1^2 / B_1} \quad (4)$$

is called ambient noise spectrum level and its values that change with the frequency and propagation conditions at sea can be found in the literature (HODGES, 2010; SALAMON, 2006; URICK, 1996).

Silent sonar echo level EL_s is equal to:

$$EL_s = SL - 2TL_s + TS, \quad (5)$$

where SL is the silent sonar transmitter's source level, $2TL_s$ are the maximal transmission losses along the transmitter – target – receiver line which will ensure the minimal assumed input echo signal-to-noise ratio TS is the target strength of the object under observation.

The level of the acoustic signal at the passive intercept sonar input EL_i is:

$$EL_i = SL - TL_i, \quad (6)$$

where TL_i are the maximal transmission losses between the silent sonar and intercept sonar, which will ensure the minimal intercept signal-to-noise ratio.

Using formulas (1), (5) and (6) we can determine the difference between the maximal transmission losses which still sustain detection for both silent and intercept sonar. It is:

$$2TL_s - TL_i = (SNR_i - SNR_s) + (NL_i - NL_s) + TS, \quad (7)$$

where the s index is used to denote silent sonar values and index i – those of the intercept sonar.

The value of the input minimal signal-to-noise ratio SNR should ensure the assumed probability of detection and false alarm. The signal-to-noise ratio at receiver output which will guarantee such probabilities is called detection threshold DT . The difference between the output and input signal-to-noise ratio depends on the type of detection and can be increased as a result of signal processing in the receiver (processing gain – PG) and array directivity (array gain – AG).

Silent sonar and intercept sonar operate under the same propagation conditions and receive the same sounding signal whether reflected from the target or a direct one. Therefore we can assume that the noise spectrum level in both systems is identical and using formulas (3) and (4) formula (7) can be written as:

$$2TL_s - TL_i = (SNR_i - SNR_s) + 10 \log \left(\frac{B_i}{B_s} \right) + TS. \quad (8)$$

The difference between transmission losses in an unlimited medium is equal to:

$$2TL_s - TL_i = 20 \log \left(\frac{R^2}{rR_1} \right) + \alpha (2R - r), \quad (9)$$

where R is the range of silent sonar r – the range of intercept sonar, $R_1 = 1 \text{ m}$, and α [dB/m] – sound absorption coefficient in water. For the assumed range R or r this equation can be solved numerically.

In subsequent chapters we will determine the minimal SNR_s values for silent sonar and SNR_i for intercept sonar with envelope detection, energy detection and spectral analysis.

3. Design, principle of operation and parameters of silent sonar

As we continue the analysis we are going to use a simplified silent sonar model whose block diagram is shown in Fig. 1. What it does not include are those elements of modern sonar that have no direct influence on detection conditions and in particular the beamformer, a common application in the majority of modern military sonar.

Silent sonar may use a variety of sounding signals with narrow autocorrelation functions (MARSZAL, SALAMON, 2013). The reason why we are going to use a signal with linear frequency modulation, is because

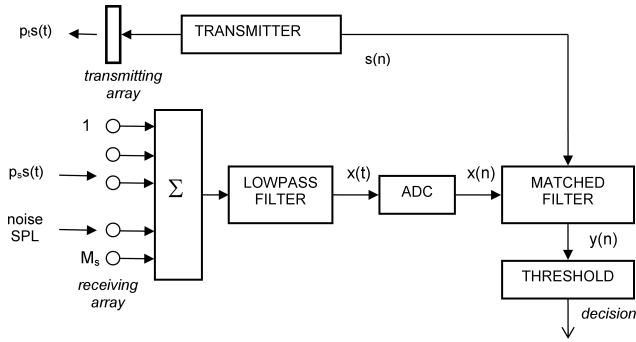


Fig. 1. Silent sonar block diagram.

other signals have similar properties for detection purposes and can be used to reduce the negative impact of Doppler effect on silent sonar operation.

Let us assume that silent sonar emits periodically repeated sounding signals with pressure p_s $s(t)$, linear frequency modulation (LFM) with carrier frequency f_0 , duration T_s and spectral bandwidth B_s . Within a single period the signal is described with the following formula:

$$s(t) = \sin \left[2\pi \left(f_0 - \frac{B_s}{2} + \frac{B_s}{T_s} t \right) t \right], \quad t \in (0, T_s). \quad (10)$$

Figure 2 shows how signal frequency changes in the function of time; its amplitude spectrum is shown in Fig. 3.

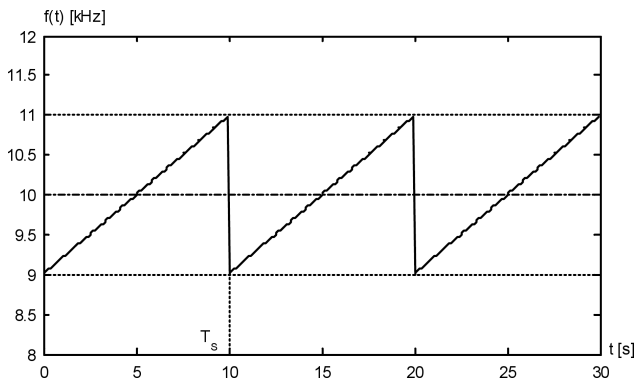


Fig. 2. Frequency of LFM signal.

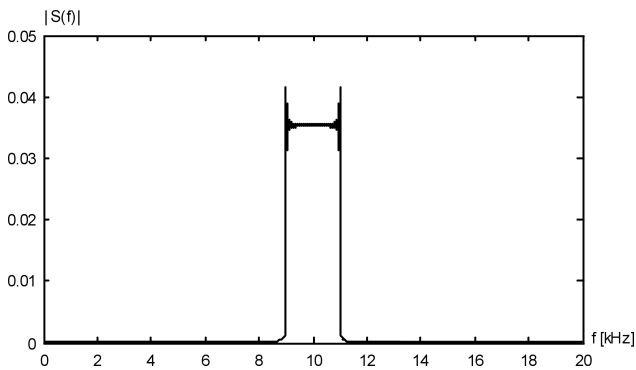


Fig. 3. Amplitude spectrum of LFM signal ($f_0 = 10$ kHz, $B_s = 2$ kHz and $T_s = 10$ s).

The amplitude of emitted signal acoustic pressure at distance $R_1 = 1$ m from the transmitting array on the axis of its beam is p_t . Incident perpendicularly on the receiving array is a wave with pressure amplitude p_s , reflected from a motionless target which is at distance R on the axis of the transmitting and receiving beam. The sonar's flat receiving array is built from M_s identical omnidirectional hydrophones, equally spaced on a rectangular surface every half wavelength for frequency f_0 . While this assumption helps formally with the analysis, it does not necessarily provide the real number of receiving channels. It is, however, explicit in determining the size of the array versus the wavelength of frequency f_0 , and its directivity. Let us assume simply, that the profile of a signal at the output of each hydrophone is a delayed copy of a sounding signal. The hydrophones also pick up the acoustic noise of the sea which in the B_s frequency band may be considered as white Gaussian noise with spectral level SPL . Electrical signals from all hydrophones are added and the summary signal following filtration in a lowpass filter with upper cut-off frequency $f_s/2$ is sampled at frequency f_s and converted into a discrete digital signal $x(n)$, where n is the sample number. Signal detection is performed in a digital matched filter to signal $s(n)$, achieved in the frequency domain.

Signal $x(n)$ is the sum of useful signal $x_s(n)$ and noise $x_n(n)$. Matched filtration is described with algorithm:

$$y(n) = \mathcal{F}^{-1} \{ X(k) \cdot S^*(k) \}, \quad (11)$$

where $X(k) = \mathcal{F} \{ x(n) \}$ and $S(k) = \mathcal{F} \{ s(n) \}$ are Fourier transforms of the signal received and transmitted, respectively. Transform $S(k)$ is calculated once and stored in the processor's memory. Transform $X(k)$ is calculated in each subsequent period T_s and all of these periods include the operations described in formula (11).

Because $x(n) = x_s(n) + x_n(n)$, we have:

$$y(n) = \mathcal{F}^{-1} \{ X_s(k) \cdot S^*(k) \} + \mathcal{F}^{-1} \{ X_n(k) \cdot S^*(k) \} = y_s(n) + y_n(n), \quad (12)$$

where $X_s(k) = \mathcal{F} \{ x_s(n) \}$ and $X_n(k) = \mathcal{F} \{ x_n(n) \}$.

Let us first determine signal $y_s(n)$ by assuming that as assumed above the acoustic wave is perpendicularly incident on the array. As a consequence, there are no time shifts between the signals at hydrophone outputs. At adder output signal amplitude increases M_s times and is equal to $p_s M_s$. At output of analogue to digital converter we get a periodical digital signal which we will write down as:

$$x_s(n) = M_s p_s [s(n - n_s) + s(n - n_s - N_s) + \dots + s(n - n_s - mN_s)], \quad (13)$$

where n_s describes echo signal delay equal to $n_s \cong 2R_s f_s / c$ (c – sound speed in water). The duration of

the sounding signal expressed with the number of samples is $N_s = T_s f_s$, and m is the period's number.

If signal duration $x(n)$ is equal to signal duration $s(n)$, the theorem of a shift in the time domain holds even though signal $x(n)$ includes fragments of adjacent periods (BRACEWELL, 2000). Formulas (11) and (12) show that:

$$y_s(n) = M_s p_s r_{ss}(n - n_s), \quad (14)$$

where $r_{ss}(n)$ is the auto-correlation function of signal $s(n)$, equal to:

$$r_{ss}(n) = F^{-1} \{|S(k)|^2\}. \quad (15)$$

The above relations occur for all subsequent periods of the sounding signal

The correlation function (20) takes on the maximal value for $n = n_s$, equal to the signal's energy. Signal power $s(n)$ just equal to 1/2, and so we have:

$$y_s(n_s) = M_s p_s N_s / 2. \quad (16)$$

Let us now determine the statistical parameters of noise at matched filter output. The variance of noise received by a single hydrophone in frequency band $f_s/2$ is equal to $N_1 \cdot f_s/2$. When the receiver's bandwidth is relatively narrow and the spaces between the hydrophones are equal to half the wavelength with frequency f_0 , the noises at array hydrophone outputs are uncorrelated. Once they are added and converted into digital form we get samples of white Gaussian noise $x_n(n)$ whose variance is equal to:

$$\sigma_M^2 = M_s N_1 N_s / 2 T_s. \quad (17)$$

Noise variance $y_n(n)$ at matched filter output can be determined from Parseval's theorem (BRACEWELL, 2000) and it is equal to:

$$\sigma^2 = N_s \sigma_M^2 / 2. \quad (18)$$

The signal-to-noise ratio DT_s at matched filter output is a consequence of formulas (1), (16), (17) and (18). It is equal to:

$$\begin{aligned} DT_s &= 10 \log \frac{[y_s(n_s)]^2}{\sigma^2} = 10 \log \left(M_s \frac{p_s^2 N_s}{N_1 f_s} \right) \\ &= 10 \log \left(M_s \frac{p_s^2 T_s}{N_1} \right) = 10 \log \left(M_s \frac{2E_s}{N_1} \right), \end{aligned} \quad (19)$$

where E_s is the energy of the signal received by a single array element. This is an extended form of a known formula which describes the signal-to-noise ratio at matched filter output (MCDONOUGH, WHALEN, 1995), and takes account of the sonar array effect.

The above formula shows that the desired signal-to-noise ratio can be maintained by reducing the sounding signal power (and at the same time, the amplitude of the signal received) and by proportionally increasing its duration T_s .

By transforming formula (19) we get:

$$\begin{aligned} DT_s &= 10 \log \left(M_s \frac{p_s^2 T_s B_s}{N_1 B_s} \right) = 10 \log \frac{p_s^2}{2 N_1 B_s} \\ &+ 10 \log M_s + 10 \log (2 B_s T_s). \end{aligned} \quad (20)$$

The expressions above are denoted as:

$$\begin{aligned} SNR_s &= 10 \log \frac{p_s^2}{2 N_1 B_s}, \\ AG_s &= 10 \log M_s, \\ PG_s &= 10 \log (2 B_s T_s) \end{aligned} \quad (21)$$

and the result is the relation we aimed to obtain: $SNR_s = DT_s - AG_s - PG_s$, which is found in formula (8).

The detection threshold $DT_s = 10 \log d_s$ is determined from operating curves of receiver ROC, for the assumed probabilities of detection PD and false alarm PFA (MCDONOUGH, WHALEN, 1995).

A programme was used to simulate the operation of silent sonar as shown in Fig. 1 and to numerically determine the signals at its output. Sonar emits a sounding signal with carrier frequency $f_0 = 10$ kHz, spectral width $B_s = 2$ kHz and duration $T_s = 10$ s, whose echo is received by a receiving transducer built from $M_s = 100$ hydrophones and sampled with frequency $f_s = 4 \cdot f_0$. The spectral noise level in frequency f_0 for sea state 4 is $SPL=50$ dB (URICK, 1996). We assume that $PD_s = 0.84$ and $PFA_1 = 3.2 \cdot 10^{-5}$ and from ROC curves we read that $DT_s = 14$ dB. Formulas (21) show that $AG_s = 20$ dB, $PG_s = 46$ dB, and $NL_s = 83$ dB. The above analysis shows that the minimal input signal-to-noise ratio $SNR_s = -52$ dB, and formula (1) shows that $EL_s = 31$ dB. We use formula (2) to determine the amplitude of pressure $p_s = 50$ μ Pa. The variance of noise received by the hydrophones is $N_1 f_s / 2 = 2 \cdot 10^9$.

Figure 4 shows an example of a signal coming from a target which is $R_s = 3$ km away from the sonar. The total of 40 000 tests helped arrive at the distribution of the density of noise probability $p(y_n)$ and the sum of

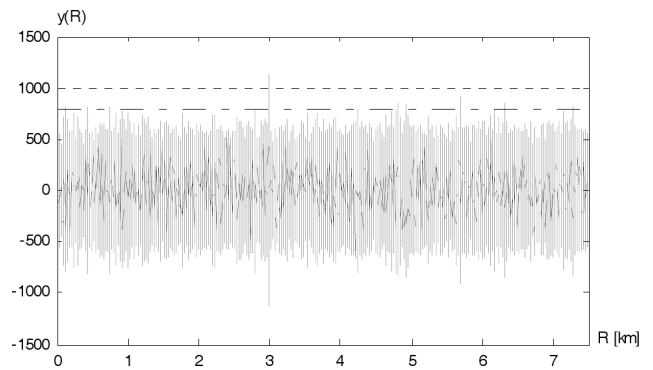


Fig. 4. Example of signal at matched filter output ($f_0 = 10$ kHz, $f_s = 40$ kHz, $B_s = 2$ kHz, $T_s = 10$ s).

signal and noise $p(y) = p(y_n + y_s)$. Distribution $p(y_n)$ was determined for a randomly selected sample $y_s(n)$, while distribution $p(y)$ – was for sample $y(n_s)$ for which function $y_s(n)$ reaches its maximum.

Figure 5 shows the distributions of probability density $99p(y_n)$ and $p(y)$, normalised for σ , and the theoretical Gaussian probability density distributions with parameters determined from formulas (16) and (18).

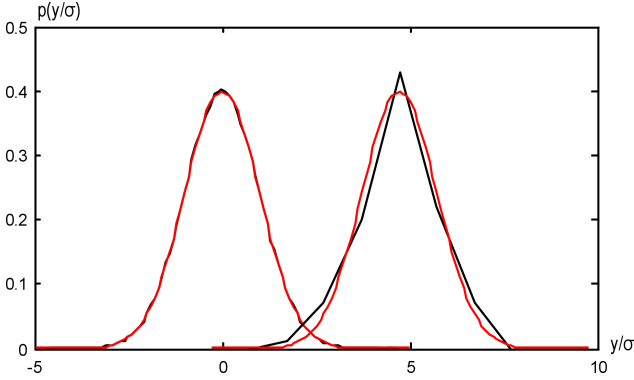


Fig. 5. Distribution of probability density of noise and signal with noise (theoretical – red line, simulation – black line).

The results of the simulations are consistent with the theoretical calculations. Because $N_s = T_s f_s = 4 \cdot 10^5$, formula (16) yields $y_s(n_s) = 10^3$. Using formula (18) we have $\sigma = 200$, and use it to determine $d_s = y_s(n_s)/\sigma = 5$. Calculated analytically from formula (19) and determined in a simulation, the output signal-to-noise ratio is equal to $DT_s = 20 \log d_s = 14$ dB. When the detection threshold $y_t = y_s(n_s) - \sigma = 800$ we obtain the above stated values of PD_s and PFA_s .

If the probability of a single noise sample exceeding the threshold is PFA_1 , then the probability of the threshold being exceeded within time T_s increases significantly and reaches 1. The average number of times the thresholds are exceeded can be estimated as $N_s \cdot PFA_1 \cong 13$ as confirmed in simulation results.

Because noise exceeds the threshold very seldom, detection performance does not suffer. These instances occur by chance and can be easily distinguished from echo signal occurring in the same (or almost the same) moment of time. The sonar monitor displays echo signals as regular lines while noise signals occur sporadically at accidental distances. As a consequence, the above stated value of $DT_s = 14$ dB can be considered an acceptable minimal signal-to-noise ratio at matched filter output.

4. Sounding signal detection in intercept sonar

4.1. Intercept sonar

Modern intercept sonars are highly developed devices which ensure optimal detection of pulse sig-

nals emitted by sonar (BOYD *et al.*, 1961; FRIEDMAN, 2006; KOTESWARA, RAO, 2006; PACE, 2009; ROSHEN *et al.*, 2009a; 2009b; SREEDAVY *et al.*, 2009; THALES-SAFARE, 2012; WARD, STEVENSON, 2000). They also help with identifying the received sonar signal bearing, tracking, measuring the operating frequency, LOFAR and DEMON type spectral analysis, etc. For the purposes of this analysis we will only look at the possibility of detecting a silent sonar signal by a hypothetical intercept sonar equipped with envelope detector, energy detector and spectrum analyser.

Figure 6 shows the model of intercept sonar discussed further in the article. With an omnidirectional beam pattern in the horizontal plane, the sonar array consists of M_i hydrophones spaced equally along a vertical straight line. Incident on the array is a plane wave with effective pressure p_i , emitted by the silent sonar transmitter. By analogy to silent sonar, the signals from the hydrophones are added and the summary signal is filtered in an anti-aliasing lowpass filter with upper cut-off frequency $f_i/2$. The signal from filter output is sampled at frequency f_i and transformed in the analogue to digital converter ADC into a digital signal $x(n)$.

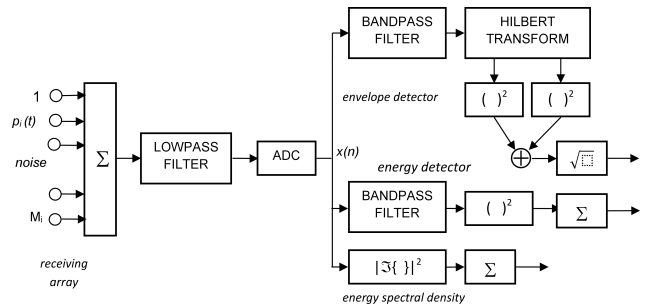


Fig. 6. Block diagram of intercept sonar.

By analogy to the silent sonar receiver, signal $x(n)$ is the sum of sounding signal $x_s(n)$ and noise $x_n(n)$. The amplitude of the sounding signal is $M_i p_i$. Because intercept sonar receives noise in a broad frequency band and the distances between the hydrophones are constant, the degree of correlation between the hydrophone output noises cannot be determined in advance. Let us accept then that the noises are uncorrelated which is an optimistic assumption from the perspective of intercept sonar and a pessimistic one if seen from the perspective of silent sonar. Noise variance $x_n(n)$ is in this case $M_i N_1 f_i/2$.

Signal $z(n)$ is processed in three detectors. They are the envelope detector, energy detector and the detector which determines energy spectral density. The decision that a sounding signal has been detected is made at detector outputs and assumes the probability of a correct decision PD_i and false alarm PFA_i .

4.2. Envelope detector

The envelope detector is designed to receive varying amplitude signals and pulse signals in conventional sonar. Because the sounding signal is continuous and has a constant amplitude, the envelope detector will only be useful if the bandpass filter meets some additional criteria. The band of the filter must wholly or partly fit into the spectrum of the sounding signal and its width B_i must be lower than that of spectrum B of the sounding signal. If these conditions are met the signal at bandpass filter output $x_f(n)$ is a pulse and periodical signal, has the sounding signal's period and may undergo envelope detection. A signal like that is shown in Fig. 7.

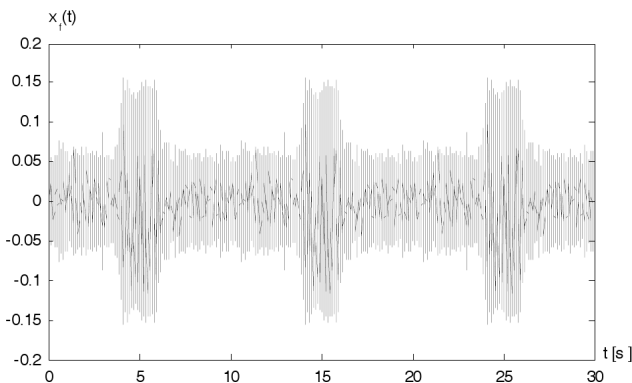


Fig. 7. Signal at bandpass filter output ($T = 10$ s, $f_0 = 10$ kHz, $B = 2$ kHz, $B_i = 0.4$ kHz).

At the output of Hilbert transform we get signal $x_f(n)$ and its quadrature component $x_q(n)$. Subsequent operations are described with formula:

$$y(n) = \sqrt{x_f^2(n) + x_q^2(n)}. \quad (22)$$

This is the envelope of a sounding signal after narrow-band filtration as exemplified in Fig. 8.

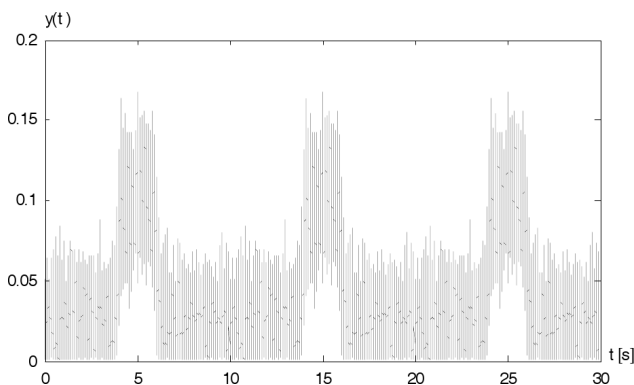


Fig. 8. Signal envelope from Fig. 7.

If all that is detected is noise, the stochastic process $y_n(n)$ is described with Rayleigh distribution (PAPOULIS, 2002). Figure 9 shows a computer-

generated distribution in an envelope detection simulation and a theoretical Rayleigh distribution.

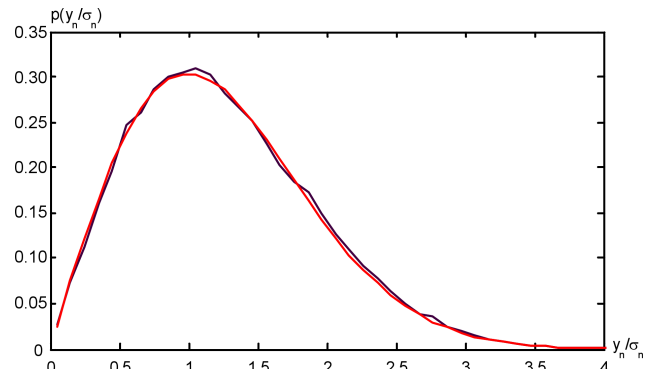


Fig. 9. Distribution of noise probability density at envelope detector output (theoretical – red line, simulation – black line) ($T = 10$ s, $f_0 = 10$ kHz, $B = 2$ kHz, $B_i = 0.4$ kHz, $SPL = 50$ dB, $M_i = 10$).

The mean value of the distribution is:

$$E[y_n(n)] = \sqrt{\frac{\pi}{2}} M_i N_1 B_i \quad (23)$$

and its variance:

$$\sigma_n^2 = \left(2 - \frac{\pi}{2}\right) M_i N_1 B_i. \quad (24)$$

When a sinusoidal signal with narrowband Gaussian noise is received the process $y(n)$ is described with the Rice distribution (PAPOULIS, 2002). When the signal-to-noise ratio is relatively high the distribution approaches Gaussian distribution as shown in Fig. 10. The black line describes the simulation-generated distribution with the red line illustrating the theoretical Gaussian distribution.

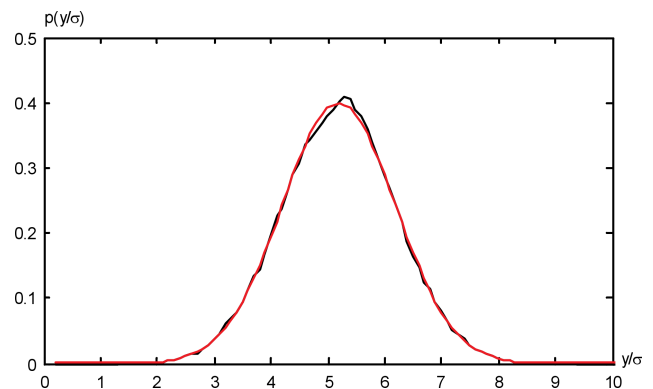


Fig. 10. Distribution (theoretical – red line, simulation – black line) of probability density of signal with noise ($p_i = 10$ mPa).

The mean value of the distribution is approximately:

$$E[y(n)] = M_i p_i \quad (25)$$

and its variance:

$$\sigma^2 = M_i N_1 B_i. \quad (26)$$

The output signal-to-noise ratio is defined as:

$$DT_i = 10 \log \frac{\{E[y(n)] - E[y_n(n)]\}^2}{\sigma^2}, \quad (27)$$

which after substituting relations (24) and (25) gives:

$$DT_i = 20 \log \left\{ \frac{E[y(n)]}{\sigma} - \sqrt{\frac{\pi}{2}} \right\}. \quad (28)$$

The signal-to-noise ratio value we are looking for may be determined numerically. As an example, for the data used to make Fig. 9 and Fig. 10, we have $E[y(n)]/\sigma = 5$, and then $DT_i = 11.5$ dB. If the detection threshold is set for $y_t = 4\sigma$ then the probability of detection is $PD_i = 0.84$. The probability of a false alarm PFA_i can be determined from the Rayleigh cumulative distribution function (PAPOULIS, 2002), as:

$$PFA_1 = \exp \left[-\frac{(4\sigma)^2}{2\sigma_n^2} \right] = \exp \left(-\frac{16}{4 - \pi} \right) = 8 \cdot 10^{-9}. \quad (29)$$

This probability relates to a single noise line which means that the probability of the threshold being exceeded in time $T = 10$ s and sampling frequency $f_i = 40$ kHz is about $3 \cdot 10^{-3}$. By reducing the output signal-to-noise ratio down to $DT_i = 8.8$ dB ($E[y(n)]/\sigma = 4$) and maintaining PD_i we increase the probability of a false alarm to $PFA_i = 2.8 \cdot 10^{-5}$ and the probable number of times the threshold will be exceeded $y_t = 3\sigma$, increases to about 11. With no a priori data about the signal received, we should assume a higher value of the output signal-to-noise ratio. Hence we have:

$$10 \log 25 = 10 \log \frac{E[y(n)]^2}{\sigma^2} = 10 \log \frac{p_i^2}{2N_1 B_i} + 10 \log M_i + 3 \text{ dB}. \quad (30)$$

The above equation for $DT_i = 11.5$ dB can be written in the form of:

$$SNR_i = DT_i - AG_i - 0.5 \text{ dB}, \quad (31)$$

where $AG_i = 10 \log M_i$. For $DT_i = 8.8$ dB the constant factor in the above formula is +0.2 dB.

By inserting $DT_i = 11.5$ dB, $AG_i = 10$ dB into formula (31) we get $SNR_i = 1$ dB.

4.3. Energy detector

We begin by determining signal y_s at energy detector output with no noise. Assuming that the spectrum of the signal received fits within the filter bandwidth of width B_i , we get:

$$y_s = M_i^2 p_i^2 \sum_{n=1}^{N_r} [s^2(n) + s^2(n - N_s) + \dots]. \quad (32)$$

The sum in the above formula is equal to the energy of signal $s(n)$, hence, we have:

$$y_s = M_i^2 p_i^2 N_i / 2, \quad (33)$$

where $N_i = T_i \cdot f_i$ is the number of added signal samples in time T_i .

Let us now move on to determine the stochastic parameters of noise at energy detector output. It is generally impossible to determine noise variances at adder output if we lack data about how the hydrophones are spaced and if the filter bandwidth is big. Let us assume approximately that the noise is uncorrelated, and then their variance at bandpass filter output is equal to:

$$\sigma_i^2 = M_i N_1 B_i. \quad (34)$$

Noise with this variance is squared and added. Noise samples can be treated as a random variable with normal distribution. As you know, the sum of squares of such a random variable has a chi-squared distribution (PAPOULIS, 2002). As stated in the central limit theorem, a distribution with a high number of added variables approaches normal distribution. The mean value of noise at adder output is:

$$E[y_n] = N_i \sigma_i^2 \quad (35)$$

and its variance is equal to:

$$\sigma_n^2 = \frac{1}{T_i B_i} N_i^2 \sigma_i^4. \quad (36)$$

Figure 11 shows the distribution of probability density of random variable y_n , as determined in the simulation. Plotted on the chart is the theoretical normal distribution with parameters determined from the formulas above. The same figure shows the distribution of random variable y , when noise is added to the sounding signal at sonar input. The calculation is made for a silent sonar sounding signal and noise with

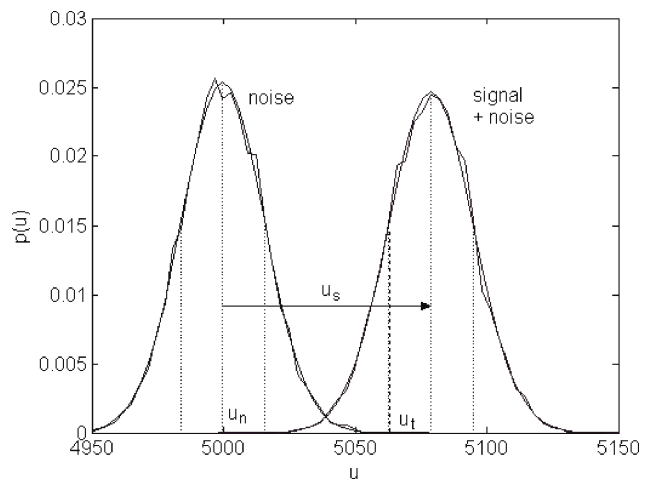


Fig. 11. Distributions of noise probability density at energy detector output.

a spectral noise level as stated above $SPL = 50$ dB. It was assumed that the number of array elements is $M_i = 10$, listening time $T_i = 5$ s, and sampling frequency $f_i = 100$ kHz. It was also assumed that the filter's mid-channel frequency is $f_0 = 10$ kHz, and its bandwidth $B_i = 10$ kHz. As a result, the filter's bandwidth covers the entire spectrum of the silent sonar signal and half of its energy during the listening phase. It was assumed that the amplitude of the signal's pressure is $p_i = 1.9$ mPa. With these parameters in place the distribution of random variable y is not much different from Gaussian distribution. The respective chart is plotted over a curve, the result of 10 000 simulated detector operations.

The distribution of the signal and noise sum has a mean value equal to $E[y] = E[y_n] + y_s$ and its variance is:

$$\sigma^2 = \sigma_n^2 + 4\sigma_i^2 y_s = \sigma_n^2 \left(1 + 4 \frac{B_i}{f_i} \frac{y_s}{E[y_n]} \right) \quad (37)$$

and is approximately equal to σ_n^2 , because $y_s \ll E[y_n]$ and $B_i < f_i$.

By using relations (27), (33), (35) and (37) we get the output signal-to-noise ratio in this form:

$$\begin{aligned} DT_i &= 10 \log \frac{\{E[y] - E[y_2]\}^2}{\sigma^2} = 10 \log \left(\frac{y_s}{\sigma} \right)^2 \\ &= 10 \log [M_i^2 \left(\frac{p_i^2}{2N_1 B_i} \right)^2 B_i T_i]. \end{aligned} \quad (38)$$

We find the logarithm and we get:

$$\frac{1}{2} DT_i = 10 \log M_i + 10 \log \left(\frac{p_i^2}{2N_1 B_i} \right) + 5 \log(B_i T_i). \quad (39)$$

Using the designation from formula (21) we have:

$$\begin{aligned} SNR_i &= 10 \log \left(\frac{p_i^2}{2N_1 B_i} \right), \\ AG_i &= 10 \log M_i, \\ PG_i &= 5 \log(B_i T_i). \end{aligned} \quad (40)$$

Formula (39) shows that the input signal-to-noise ratio is equal to:

$$SNR_i = \frac{1}{2} DT_i - AG_i - PG_i. \quad (41)$$

Given the data we used to make Fig. 11 we have: $DT_i = 20 \log(y_s/\sigma) = 20 \log 4 = 12$ dB, $AG_i = 10$ dB, $PG_i = 5 \log(5 \cdot 10^4) = 23.5$ dB. The input signal-to-noise ratio is then equal to $SNR_i = -27.5$ dB. With the detection threshold equal to $y_t = E[y] - \sigma$ we have $PD_i = 0.84$ and $PFA_i = 1.3 \cdot 10^{-3}$.

One could say that the DT_i value we assumed is sufficient or even too high because PFA_i relates in this case to the entire time the signal is added, so it could be

much higher. By the same token the required signal-to-noise ratio could be lower, if the spectral noise density were known and did not change during listening. In practice these conditions are difficult to meet because spectral density of noise can only be measured (identify $E[y_n]$ value) in the absence of silent sonar signal, which in this case is continuous.

To understand the effects of misestimating the spectral density of noise on detection conditions, let us assume that in the example above spectral density of noise increased by 1% or decreased by 1%. The effects of the changes are shown in Fig. 12 and Fig. 13. The black line represents the distributions of probability density for the above example and the blue line shows the distributions after spectral density of noise has changed.

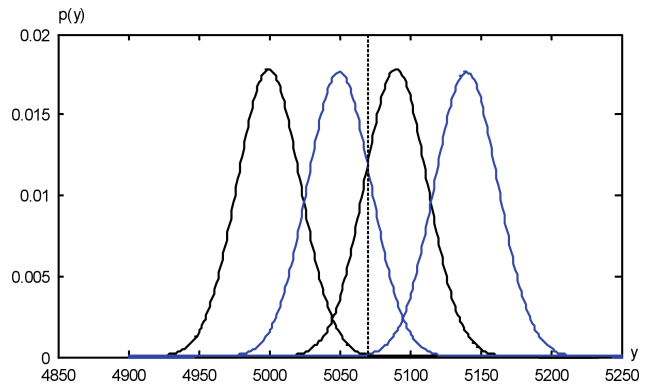


Fig. 12. Effect of an increase in noise spectral density.

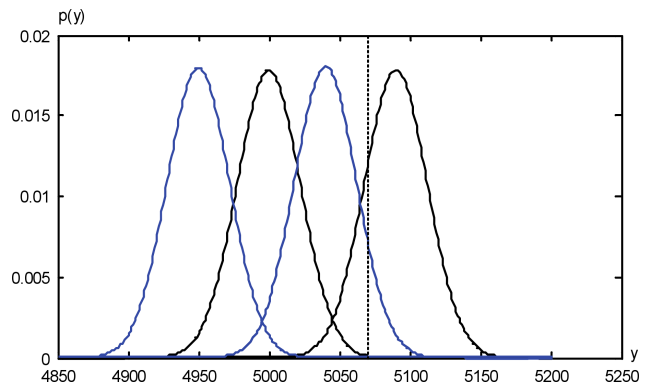


Fig. 13. Effect of a decrease in noise spectral density.

As you can see in Fig. 12, an increase in spectral density of noise increases detection probability and the probability of false alarm. As spectral density of noise continues to increase slightly PFA_i quickly approaches unity. As shown in Fig. 13 a reduction in spectral density of noise causes PD_i and PFA_i to go down to nearly a zero. In both cases a slight change in noise level like this deteriorates detection conditions to an unacceptable level.

To prevent this effect from happening, DT_i must be raised high enough for PD_i not to drop below the assumed value, and for PFA_i not to exceed the accept-

able level. To determine the desired DT_i let us assume that spectral density of noise changes by $\pm qN_1$. Formulas (34) and (35) show that when noise level increases its mean value is $(1 + q)E[y_n]$ and $(1 - q)E[y_n]$ when it drops. The change in its variance is so small, amounting to $(1 + q)^2\sigma_n^2$ and $(1 - q)^2\sigma_n^2$ respectively (formula (37)) that it is of no practical significance. Let us assume that detection occurs when threshold y_t is exceeded. In addition let us assume that minimal value $PD_i \cong 0.84$, and that the maximal value $PFA_i = 1.3 \cdot 10^{-3}$. The first assumption is met when $y_t = E[y_n] + y_s\sigma$, and the second when $y_t = E[y_n] + 3\sigma$. For a growing mean value of noise, the detection threshold at which PFA_i has the desired value is $y_t = E[y_n](1 + q) + 3\sigma$. When the mean value of noise drops, the desired value PD_i is ensured for threshold $y_t = E[y_n](1 - q) + y_s\sigma$. By solving these equations, we get:

$$y_s = 2qE[y_n] + 4\sigma. \tag{42}$$

The above relation shows that the minimal value of the detection threshold is:

$$\begin{aligned} DT_i &= 20\log\frac{y_s}{\sigma} = 20\log\left[2q\frac{E[y_n]}{\sigma} + 4\right] \\ &= 20\log\left[2q\sqrt{T_i B_i} + 4\right]. \end{aligned} \tag{43}$$

Please note that when $q = 0$ we get $DT_i = 12$ dB, which is the value achieved in the example illustrated in Fig. 11. Because spectral density of noise fluctuates, the detection threshold must be increased as well as the input signal-to-noise ratio. As an example, when SPL changes by 1 dB ($q = 0.25$), for $T_i = 5$ s and $B_i = 10$ kHz, the required detection threshold is $DT_i = 41.2$ dB, which causes the input signal-to-noise ratio to increase $SNR_i = -12.9$ dB.

Analogous fluctuations of noise levels in silent sonar do not cause any significant deterioration of detection conditions. A lower spectral density of noise N_1 increases PD_s which is good and reduces PFA_s , and when it is higher – PD_s goes down slightly and the increase in PFA_s is minor as well.

4.4. Spectral analysis

Initial signal processing in this system is performed just as in intercept sonar with envelope detection and energy detection. Afterwards a calculation is made of discrete Fourier transform $X(k)$, and then of energy spectral density $Y(k) = |X(k)|^2$.

Subsequent figures show the characteristic shapes energy spectral density of the sounding signal from silent sonar without noise. Because the duration of the signal is not known, in intercept sonar the listening time is usually different from that period. Energy spectral density as shown in Fig. 14 is characteristic of cases when observation time T_i is lower than period T_s and fits into it entirely. In other situations the

spectrum of the signal received consists of its separate fragments as exemplified in Fig. 15 and Fig. 16. All the energy spectral density charts were made for the following data: $f_0 = 10$ kHz, $T = 10$ s, $p_i = 0.1$ mPa, $M_i = 10$, $f_i = 40$ kHz.

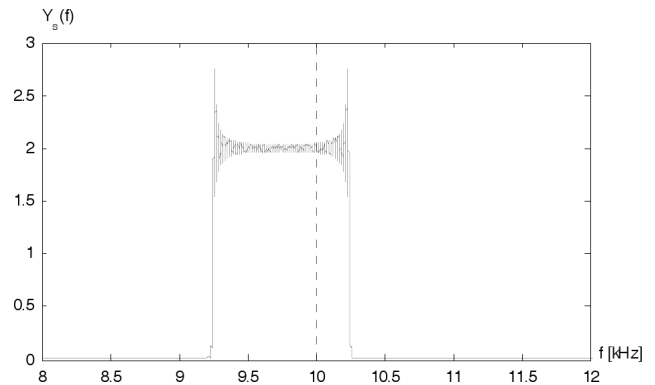


Fig. 14. Energy spectral density ($T_i = 5$ s).

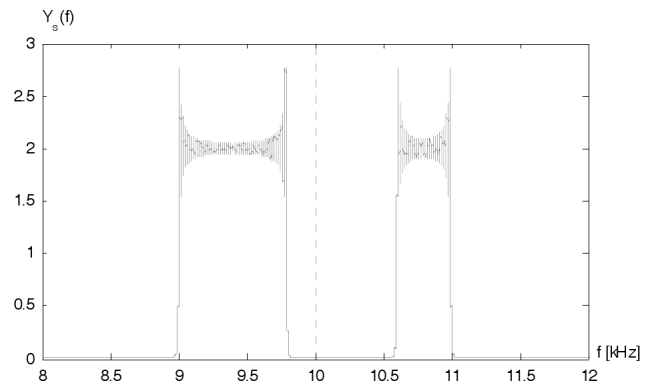


Fig. 15. Energy spectral density ($T_i = 6$ s, range of observation in two periods).

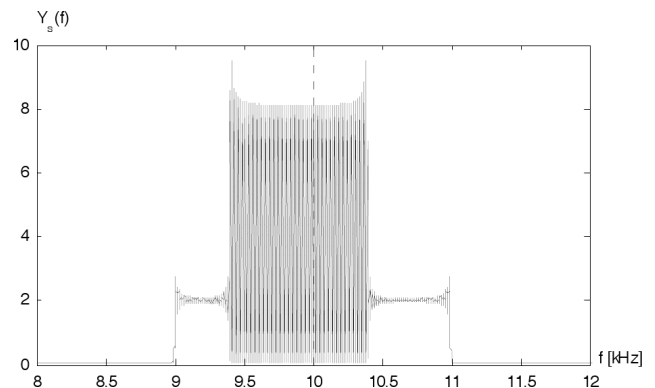


Fig. 16. Energy spectral density ($T_i = 15$ s).

Further in the analysis we will only consider a case when Fourier transform is calculated in time interval T_i fitting into a single sounding signal period T , (Fig. 14). Please note: this assumption is not always met for shorter range silent sonar. Figure 17 shows energy spectral density when a sounding signal with pressure $p_i = 50$ mPa is received with noise whose spectral density is $N_1 = 10^{-7}$ (re 1 Pa). The calculations were

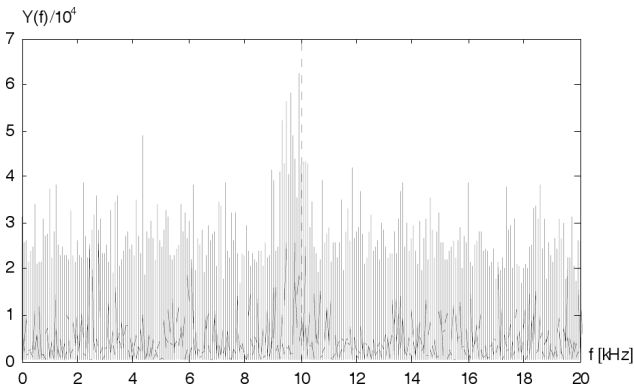


Fig. 17. Energy spectral density of signal with noise.

made based on data from Fig. 14. The input signal-to-noise ratio in the band $f_i/2$ is $SNR_i = -22$ dB.

To calculate the necessary values in the range equation, we will take the same steps as in the previous sections.

Figure 18 shows the probability density distributions of the height of energy spectral density lines for noise. As you can see, the distribution we have obtained in the numerical experiment is no different from the theoretical exponential distribution. Figure 19 shows the experimental probability density

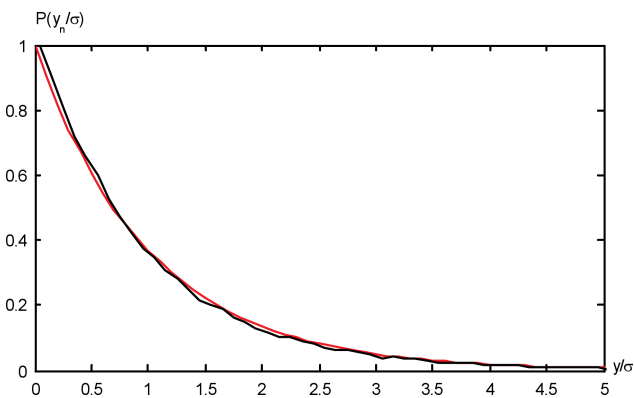


Fig. 18. Probability density distribution of the height of energy spectral density lines of noise (theoretical – red line, simulation – black line).

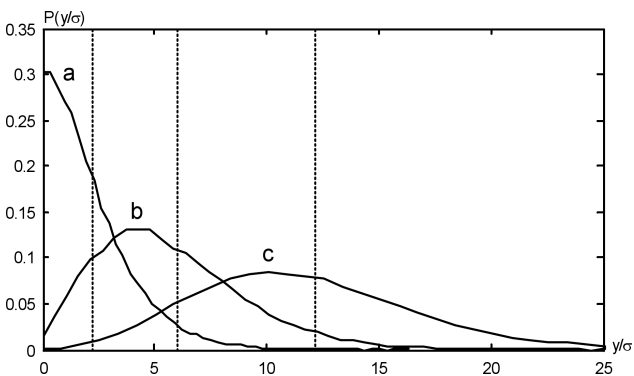


Fig. 19. Probability density distribution of the height of energy spectral density lines of signal with noise SNR_i : a) 22 dB, b) 16 dB, c) 12 dB.

tributions of the height of energy spectral density lines for a signal received with noise. All the charts were made for noise whose probability density distribution was shown in Fig. 18. The amplitude of the received sounding signal is the parameter, in other words, the input signal-to-noise ratio SNR_i .

The probability density distribution of the height of energy spectral density lines for white noise is exponential and its mean value is equal to standard deviation σ , which is:

$$E[Y_n] = \sigma = \frac{1}{2} M_i N_1 f_i^2 T_i. \quad (44)$$

The mean value of the height of energy spectral density lines of a signal without noise is equal to:

$$E[Y_s] = \frac{1}{4} M_i^2 p_i^2 f_i^2 \frac{T_s}{B_s} \quad (45)$$

and of a signal with noise, it is the sum of the mean values, namely:

$$E[Y] = E[Y_s] + E[Y_n]. \quad (46)$$

The variance of the distribution in question is approximately equal to:

$$\sigma_y^2 \cong \sigma^2 + 2\sigma E[Y_s]. \quad (47)$$

Formulas (44), (45) and (46) show that output signal-to-noise ratio defined in formula (27) is:

$$\begin{aligned} DT_i &= 10 \log \frac{E[Y_s]^2}{\sigma^2} = 20 \log \frac{1}{2} \frac{M_i p_i^2 T_s}{N_1 B_s T_i} \\ &= 20 \log \frac{M_i p_i^2 T_s f_i}{(N_1 f_i)(2 B_s T_i)}. \end{aligned} \quad (48)$$

Please note that a possibly low output signal-to-noise ratio is what works best for silent sonar. To achieve this the signal generated should have a high B_s/T_s ratio. Intercept sonar, on the other hand, prefers a short observation time T_i . This, however, will generate narrow fragments of the sounding signal spectrum appearing on different frequencies in the subsequent observation periods which may impede their visual detection.

After we find the logarithm and set the designations:

$$\begin{aligned} SNR_i &= 10 \log \left(\frac{p_i^2}{N_1 f_i} \right), \\ AG_i &= 10 \log M_i, \\ PG_i &= 10 \log \left(\frac{f_i T_s}{2 B_s T_i} \right), \end{aligned} \quad (49)$$

we can calculate the input signal-to-noise ratio for the spectral analysis case using the formula (41).

While it is theoretically possible to determine the minimal output signal-to-noise ratio DT_i from the assumed detection probability PD_i and acceptable probability of false alarm PFA_i using the usual procedure, it does not offer any practical benefits. The mean value

of the height of energy spectral density lines described with formula (45) depends on unknown parameters of the signal received T_s and B_s . In addition, threshold detection does not yield clear-cut results. Probabilities PD_i and PFA_i determined from probability distributions shown in Fig. 18 and Fig. 19 only apply to individual spectral lines, which means that the probabilities referring to the entire time of observation T_i depend on the number of spectral lines. Determining the probability of false alarm is explicit because the number of noise spectral lines is constant. Detection probability, on the other hand, cannot be determined if we do not know in advance the spectral width of the signal received.

Figure 17 shows that visual observation of the spectrum, in particular on presentations with waterfall history records makes it fairly easy to distinguish the spectrum of the signal from the background of noise spectrum even if the output signal-to-noise ratio is low (in Fig. 17 $DT_i = 2$ dB). This is not only because individual spectral lines are higher, but because they are concentrated in a specific frequency band. This kind of concentration can be clearly seen in the running sum of spectral lines height less the trend line, namely:

$$Z(n) = \sum_{k=1}^n Y(k) - \beta n, \quad n = 1, 2, \dots, N_i, \quad (50)$$

where $N_i = f_i T_i$ and

$$\beta = \frac{\sum_{n=1}^{N_i} \left\{ n \left[\sum_{k=1}^n Y(k) \right] \right\}}{\sum_{n=1}^{N_i} n^2}. \quad (51)$$

Figure 20 shows function $Z(f)$ determined from the spectrum in Fig. 17. As you can see, signal detection is much more likely here as opposed to direct observation of the signal's energy spectral density.

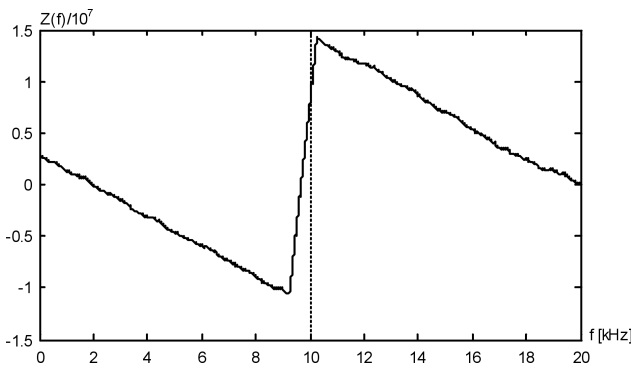


Fig. 20. Running sum of spectral lines height with trend removed ($SNR_i = -22$ dB).

As a consequence, the input signal-to-noise ratio may be reduced as illustrated in Fig. 21 and Fig. 22. Figure 21 shows the energy spectral density for the sounding signal's parameters and the receiver from

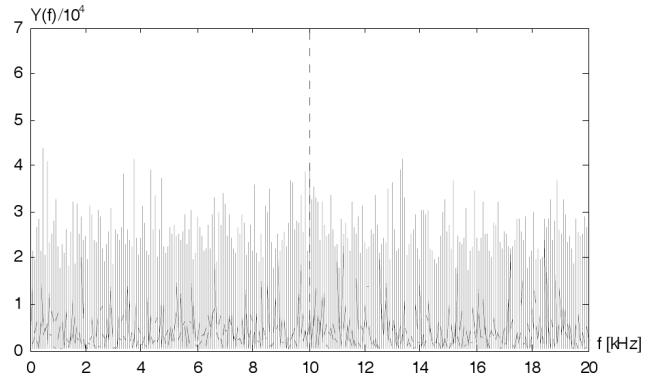


Fig. 21. Energy spectral density of signal with noise for $SNR_i = -32$ dB.

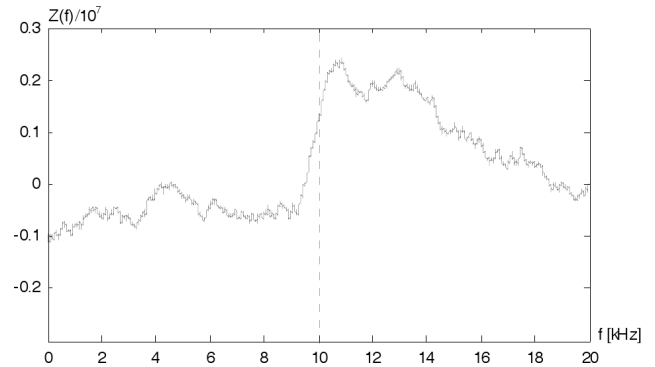


Fig. 22. Running sum of spectral lines height with trend removed ($SNR_i = -32$ dB).

Fig. 17. The input signal-to-noise ratio is reduced by 10 dB to reach $SNR_i = -32$ dB. The output signal-to-noise ratio went down from +2 dB to -18 dB, which is a direct result of formula (50).

The output signal-to-noise ratio of the process $Z(n)$ is defined as $DT_i = 20 \log(\Delta Z / \sigma_z)$. Amplitude ΔZ for the signal alone shown in Fig. 20, is equal to:

$$\Delta Z = E[Y_s] B_i T_i. \quad (52)$$

The variance of noise can be determined from the empirically obtained approximate formula:

$$\sigma_z^2 \cong \frac{1}{16} \sigma^2 f_i T_i. \quad (53)$$

Using formulas (45) and (46) we get:

$$DT_i = 10 \log \frac{\Delta Z^2}{\sigma_z^2} = 10 \log \left[4 \left(\frac{M_i p_i^2}{N_1 f_i} \right)^2 T_i f_i \right]. \quad (54)$$

By denoting:

$$\begin{aligned} SNR_i &= 10 \log \left(\frac{p_i^2}{N_1 f_i} \right), \\ AG_i &= 10 \log M_i, \\ PG_i &= 5 \log(4 T_i f_i). \end{aligned} \quad (55)$$

we determine once again the components found in formulas (41).

In the example shown in Fig. 22, the output signal-to-noise ratio is $DT_i \cong 15$ dB which makes it easy to distinguish from noise. The assumption in the example is that $T_i = 5$ s, $f_i = 40$ kHz and $M_i = 10$, and from there that $AG_i = 10$ dB and $PG_i = 29.5$ dB. Formula (41) gives $SNR_i = 7.5 - 10 - 29.5 = -32$ dB. The same value of the input signal-to-noise ratio was arrived at in the simulation by assuming that $p_i = 1.6$ mPa, $SPL = -7$ dB/re 1 Pa and bandwidth $f_i/2 = 20$ kHz.

5. Intercept sonar and silent sonar ranges

The range of intercept sonar r means the maximal distance to silent sonar at which the intercept sonar detects the silent sonar's sounding signal. The criterion of sounding signal detection is the minimal output signal-to-noise ratio DT_i which is usually determined from assumed probabilities of detection PD_i and false alarm PFA_i .

The range of silent sonar R is the maximal target distance with target strength TS , at which the silent sonar detects the echo signal from the target with assumed probability of detection PD_s and false alarm PFA_s .

The relation between the two ranges is described in formulas (8) and (9) and is the result of the difference in input signal-to-noise ratios SNR_s and SNR_i , bandwidths B_s and B_i in the receivers of both systems and target strength TS . The input signal-to-noise ratio is a function of the sounding signal's parameters, receiver parameters and the detection method applied. And so by using formulas (21), (31), (41) and (55) consecutively after elementary transformations, we have:

- for intercept sonar with envelope detection

$$2TL_s - TL_i = (DT_i - DT_s) + 10 \log \frac{M_s}{M_i} + 10 \log(B_i T_s) + TS + 2.5 \text{ dB}, \quad (56)$$

- for intercept sonar with energy detection

$$2TL_s - TL_i = \left(\frac{1}{2} DT_i - DT_s \right) + 10 \log \frac{M_s}{M_i} + 5 \log(B_i T_s^2 / T_i) + TS + 3 \text{ dB}, \quad (57)$$

- for intercept sonar with spectral analysis

$$2TL_s - TL_i = \left(\frac{1}{2} DT_i - DT_s \right) + 10 \log \frac{M_s}{M_i} + 5 \log(T_s^2 f_i / T_i) + TS - 3 \text{ dB}. \quad (58)$$

The derivation of the last relation takes into account the fact that noise band B_i in formula (8) is equal to $f_i/2$.

Silent sonar will benefit from a possibly high value of the left side of the above equations. This can be achieved by increasing the number M_s of array elements (reducing beam width) and extending the period T_s of the sounding signal. While the spectrum width B_s of the sounding signal has no direct impact on the relation between the range of the two sonars, keeping it high is good for silent sonar range resolution. It also means that a wide band must be used in intercept sonar, which increases the difference between transmission losses.

The range of intercept sonar can be extended (the left side of the above equations can be reduced) by increasing the number M_i of array elements, although there is a limitation due to the desired and high beam width. What also works well is a low band width of B_i and long observation time T_i . There are, however, some limitations, because band B_i must overlap with band B_s of the sounding signal.

The relations between intercept sonar and silent sonar ranges can be determined through a numerical solution of Eqs. (9) and (56), (57) and (58) for specific parameters of both systems and for a known absorption coefficient (AINSLIE, 1998), found in formula (9). Presented below are examples of such solutions which help arrive at more general conclusions. To that end we are going to investigate three classes of silent sonar, namely long-range sonar with operating frequency $f_0 = 10$ kHz, medium-range sonar with operating frequency $f_0 = 40$ kHz and short-range sonar with operating frequency $f_0 = 100$ kHz. We will also assume that each sonar has an array whose square surface consists of $M_s = 20 \times 20 = 400$ elements spaced equally every half wavelength for frequency f_0 . The array's beam width is 5° in both sections. Table 1 gives these and other silent sonar parameters. The tables also includes the values of logarithmic absorption coefficient in the ocean, Baltic and fresh water for the sonar operating frequencies as stated above.

Table 1. Parameters of silent sonar.

Carrier frequency	DT_s	Number of array elements	Period of sounding signal	Signal spectral width	Absorption coefficient α		
					Ocean	Baltic	Fresh water
f_0 [kHz]	[dB]	M_s	T_s [s]	B_s [kHz]	[dB/km]	[dB/km]	[dB/km]
10	14	400	20	2	0.98	0.25	0.034
40	14	400	5	8	11.2	2.7	0.58
100	14	400	2	20	34.0	9.5	3.64

The parameters of intercept sonar were selected arbitrarily under the assumption that the sonar can receive signals in a specific number of channels with fixed frequency bands. It was assumed that for envelope detection band width $B_i = 0.5 \cdot B_s$, for energy detection $B_i = 4 \cdot B_s$, and for spectral analysis $B_i = 0.5 \cdot f_i$. It was assumed that sampling frequency $f_i = 400$ kHz, and observation time is $T_i = 10$ s. The sonar has a vertical linear array consisting of $M_i = 10$ elements which ensures a certain noise reduction depending on the listening band and the spacing between its elements.

It was assumed that the long-range sonar range applies to target detection that has target strength $TS = 0$ dB, medium-range – $TS = -10$ dB and short range – $TS = -20$ dB. Using the above data and values DT_i derived in the previous section from formulas (56), (57) and (58), the differences in transmission losses were calculated and put in Table 2.

Table 2. Difference in transmission losses $2TL_s - TL_i$ [dB] for silent sonar with parameters as defined in Table 1.

Carrier frequency	Envelope detection	Energy detection	Spectral analysis
	$DT_i = 11.5$ dB	$DT_i = 41.2$ dB	$DT_i = 15$ dB
10 kHz	59.0	53.1	42.5
40 kHz	49.0	40.1	26.2
100 kHz	39.0	28.1	12.5

What makes silent sonar useful is the extended distance r , at which the intercept sonar detects sounding signals from pulse sonar which emit “ping” constant frequency signals or “chirp” signals with linear frequency change. In these sonars envelope detection was applied when receiving “ping” signals and matched filtration when receiving “chirp” signals. As regards “chirp” signals it was assumed that in pulse sonar pulse duration is 40 times shorter than given in Table 1. Formulas (56), (57) and (58) show that transmission loss differences $2TL_s - TL_i$ are now 16 dB lower than shown in Table 2. The values for the “ping” signal were calculated from formula (8) by inserting $SNR_s = DT_s 10 \log(M_s) - 0.5$ dB ($DT_s = 11.5$ dB) and using relations (31), (41) and (55) which refer to intercept sonar. Table 3 gives the parameters for which the calculations were made and their results. It was also assumed that $T_i = 10$ s, and $f_i = 400$ kHz.

Table 3. Difference in transmission losses $2TL_s - TL_i$ [dB] for pulse sonar with “ping” and “chirp” type signals.

Carrier frequency	T_s [s]	B_s [kHz]	B_i [kHz]	“chirp”			“ping”		
				Envelope detection	Energy detection	Spectral analysis	Envelope detection	Energy detection	Spectral analysis
10 kHz	0.5	0.4	1	43.0	37.1	28.5	20.0	9.6	3.5
40 kHz	0.1	1.6	4	33.0	24.1	10.2	10.0	-3.4	-12.5
100 kHz	0.05	4	10	23.0	12.1	-3.5	2.2	-13.2	-24.3

The figures below show the intercept sonar range r in the function of silent sonar range R . To compare, each figure comes with another figure with analogous charts for pulse sonar emitting “ping” and “chirp” signals. The figures are grouped into sonar classes with identical distances for the individual classes to help with comparing the results. The relevant parameters are given in the Tables above.

Four consecutive figures are for the long-range sonar ($f_0 = 10$ kHz). Figure 23 shows the ranges of intercept sonar receiving silent sonar sounding signals in oceanic water and receiving pulse sonar sounding signals under the same conditions in Fig. 24. Analogous relations for sonar performance in the Baltic are given in Fig. 25 and Fig. 26. These and other figures use the letter a to mark the range of intercept sonar with spectral analysis, the letter b – with energy detec-

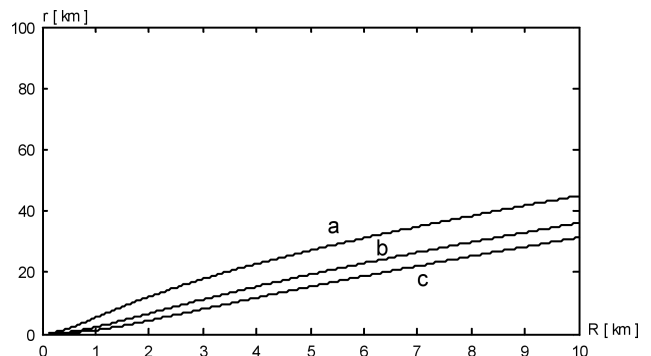


Fig. 23. Intercept ranges of long-range silent sonar in the ocean (a – spectral analysis b – energy detection, c – envelope detection).

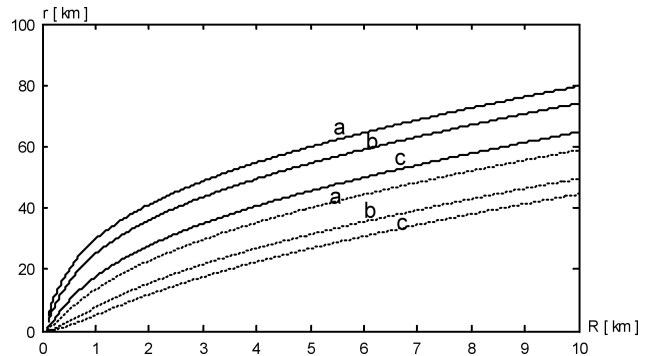


Fig. 24. Intercept ranges of long-range pulse sonar in the ocean (solid line – “ping” signal, dotted line – “chirp” signal).

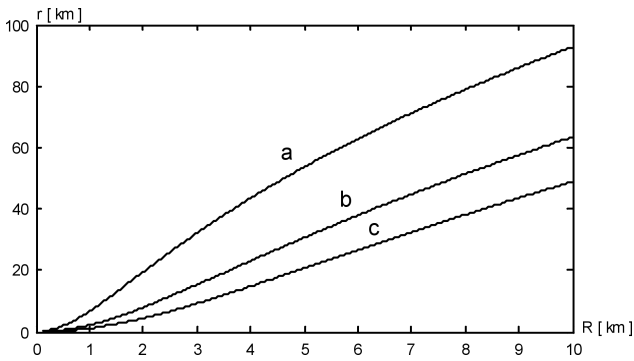


Fig. 25. Intercept ranges of long-range silent sonar in the Baltic.

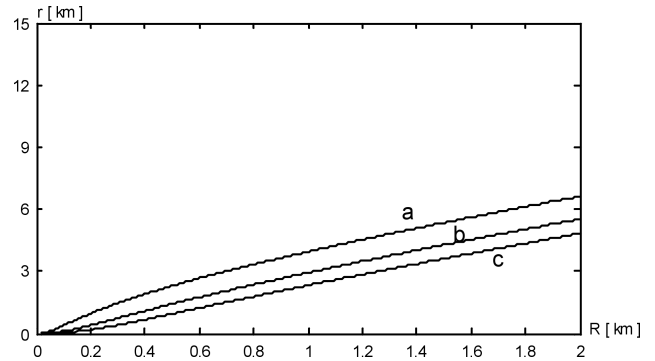


Fig. 27. Intercept ranges of medium-range silent sonar in the ocean.

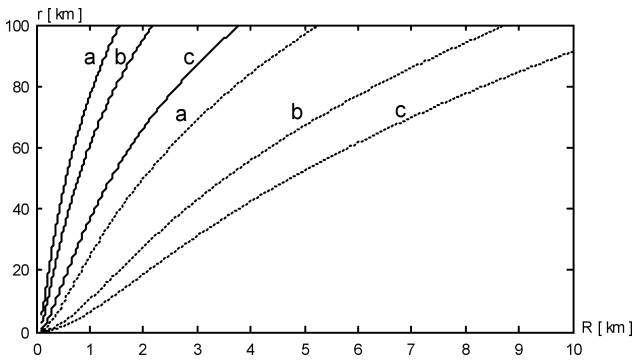


Fig. 26. Intercept ranges of long-range pulse sonar in the Baltic.

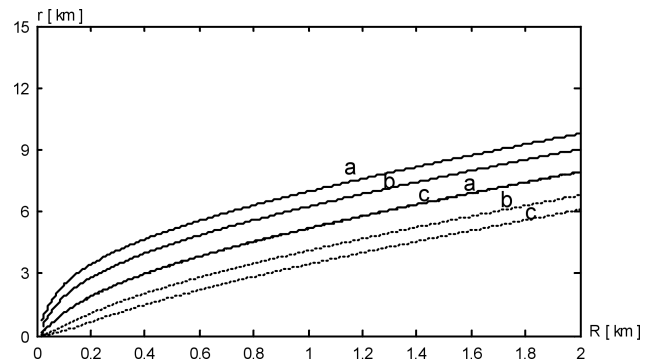


Fig. 28. Intercept ranges of medium-range pulse sonar in the ocean.

tion, and the letter *c* – with envelope detection. Pulse sonar figures use a solid line to mark the ranges of intercept sonar receiving “ping” sounding signals and a dotted line to mark “chirp” sounding signals.

The following general conclusions can be drawn from the figures:

- Irrespective of the detection method used in intercept sonar, it always detects silent sonar sounding signals from a shorter distance than it does pulse sonar sounding signals.
- Spectral analysis helps to achieve longer intercept ranges in the case of both silent sonar and pulse sonar sounding signals.
- The ranges of intercept sonar are much longer in low salinity water, e.g. in the Baltic, than in the ocean due to lower absorption.

The next four figures show the ranges of intercept sonar receiving echo signals from medium-range sonars. Because they operate at a higher frequency, absorption is stronger which leads to shorter ranges as opposed to low frequency sonar. To take account of this fact the ranges of silent sonar, pulse sonar and intercept sonar were reduced

When we analyse this group of figures we can see that the general conclusions on long-range sonar apply to medium-range sonar as well. In addition, it should be noted that an increase in absorption reduces slightly

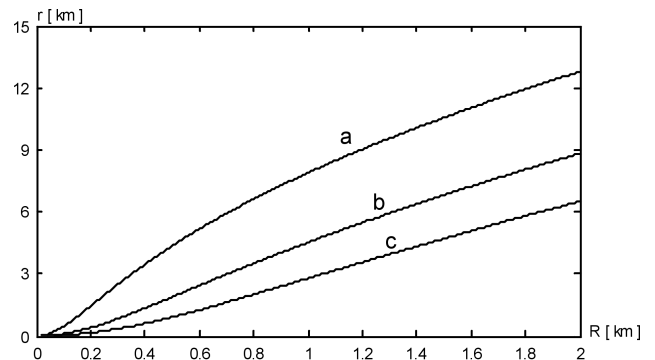


Fig. 29. Intercept ranges of medium-range silent sonar in the Baltic.

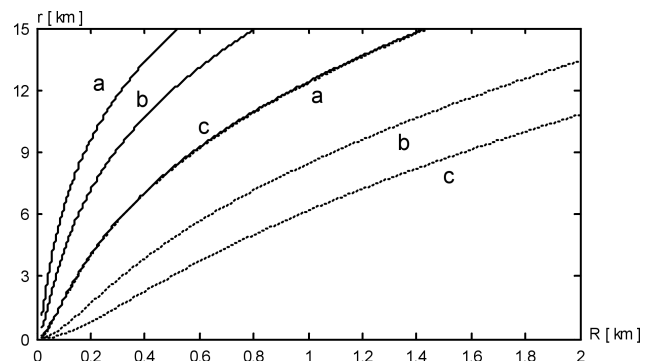


Fig. 30. Intercept ranges of medium-range pulse sonar in the Baltic.

the effects of silent sonar and pulse sonar parameters on intercept sonar ranges.

The next six figures cover short-range sonar. Because such a sonar is also used in inland fresh water the relevant ranges are also included.

The above series of figures confirms the conclusion regarding the strong effect absorption has on detection ranges of signals emitted by both silent sonar and pulse sonar. The most important conclusion is also verified which is that silent sonar sounding pulses are always detected by intercept sonar from a distance which is shorter than in the case of comparable pulse sonars.

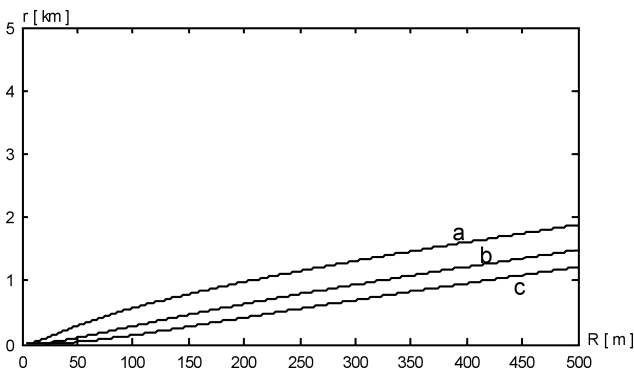


Fig. 31. Intercept ranges of short-range silent sonar in the ocean.

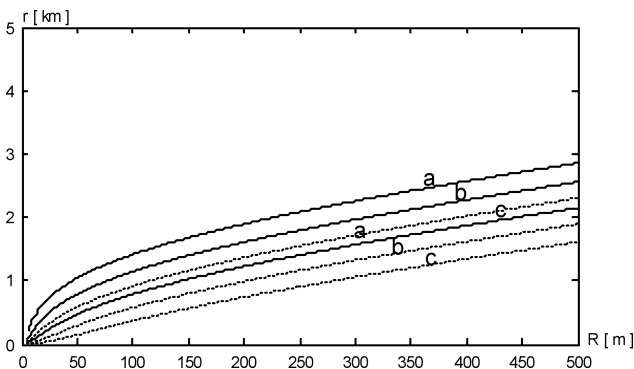


Fig. 32. Intercept ranges of short-range pulse sonar in the ocean.

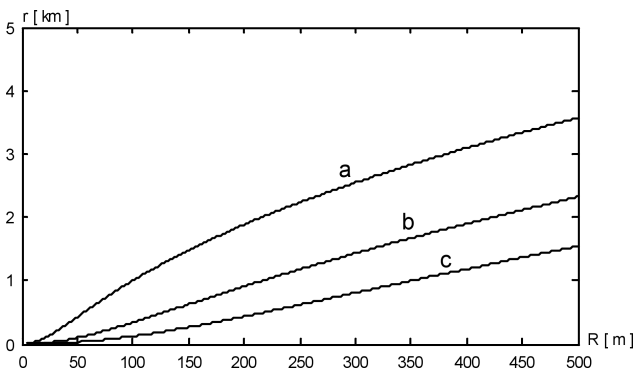


Fig. 33. Intercept ranges of short-range silent sonar in the Baltic.

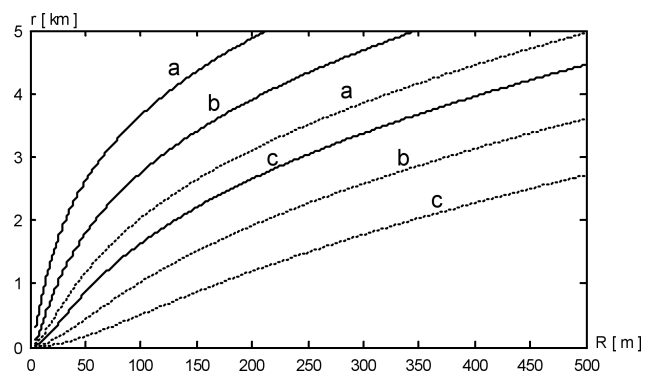


Fig. 34. Intercept ranges of short-range pulse sonar in the Baltic.

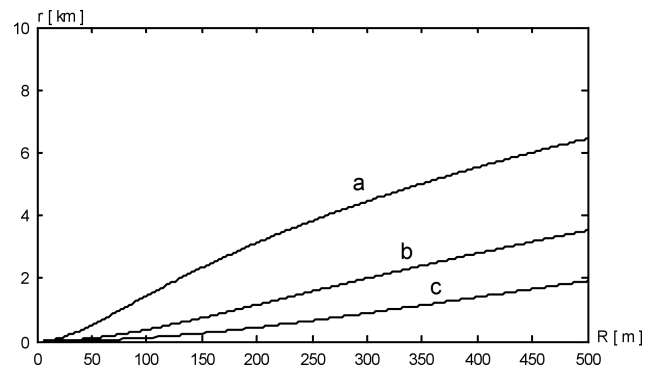


Fig. 35. Intercept ranges of short-range silent sonar in inland waters.

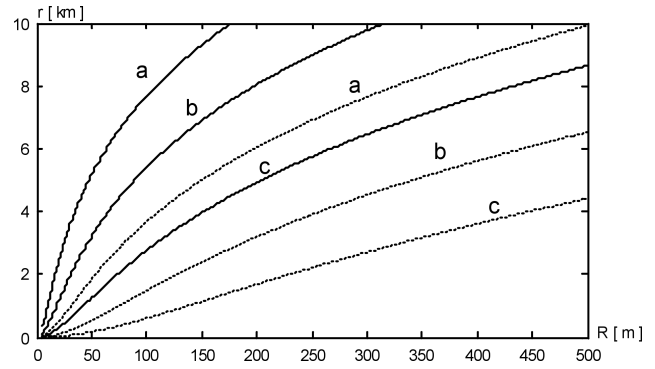


Fig. 36. Intercept ranges of short-range pulse sonar in inland waters.

6. Summary

Our analysis of the silent sonar CWFM sounding signal intercept range shows that silent sonar application makes sense where stealth is required. Derived for the purposes of the analysis, the formulas help numerically analyse the efficiency and stealth of operation of new designs of silent sonar. They also help with optimising the parameters of silent sonar for specific applications.

On the other hand, the methods and relations described in the article can also be helpful with designing and optimising signal processing methods in intercept sonar.

References

1. AINSLIE M.A., MCCOLM J.G. (1998), *A Simplified Formula for Viscous and Chemical Absorption in Sea Water*, Journal of the Acoustical Society of America, **103**, 3, 1671–1672.
2. BOYD J.A., HARRIS D.B., KING D.D., WELCH H.W. (1961), *Electronic Countermeasures, Section 23.5: Interception*, Institute of Science and Technology of The University of Michigan for the U.S. Army Signal Corps under Contract DA-36-039 SC-71204.
3. BRACEWELL R.N. (2000), *The Fourier Transform and its Applications*, (Third Edition), McGraw-Hill.
4. FRIEDMAN N. (2006), *The Naval Institute Guide to World Naval Weapon Systems*, Naval Institute Press.
5. FULLER K.L. (1990), *To See and not Be Seen*, IEE Proceedings-F, **137**, 1, 1–10.
6. GRELOWSKA G., KOZACZKA E., KOZACZKA S., SZYM-CZAK W. (2013), *Underwater Noise Generated by a Small Ship in the Shallow Sea*, Archives of Acoustics, **38**, 3, 351–356.
7. HODGES R.P. (2010), *Underwater Acoustics: Analysis, Design and Performance of Sonar*, John Wiley & Sons, Ltd.
8. KOTESWARA RAO S. (2006), *Pseudo Linear Kalman Filter For Underwater Target Location Using Intercept Sonar Measurements*, Proceedings of IEEE/ION PLANS, San Diego, 1036–1039.
9. KOZACZKA E., GRELOWSKA G. (2004), *Shipping noise*, Archives of Acoustics, **29**, 2, 169–176.
10. KOZACZKA E., DOMAGALSKI J., GRELOWSKA G., GLOZA I. (2007), *Identification of hydro-acoustic waves emitted from floating units during mooring tests*, Polish Maritime Research, **14**, 4, 54, 40–46.
11. KOZACZKA E., GRELOWSKA G. (2011), *Shipping low frequency noise and its propagation in shallow water*, Acta Physica Polonica A, **119**, 6A, 1009–1012.
12. McDONOUGH R.N., WHALEN A.D. (1995), *Detection of Signals in Noise*, (Second Edition), Academic Press.
13. MARSZAL J. (2014), *Experimental Study of Silent Sonar*, Archives of Acoustics, **39**, 1, 103–115.
14. MARSZAL J., SALAMON R. (2012), *Distance Measurement Errors in Silent FM-CW Sonar with Matched Filtering*, Metrology and Measurement Systems, **XIX**, 2, 321–332.
15. MARSZAL J., SALAMON R. (2013), *Silent Sonar for Maritime Security Applications*, Proceedings of Meetings on Acoustics, Acoustics Society of America, 2013, **17**, 070082.
16. MARSZAL J. (1992), *Directivity Pattern of Active Sonars with Wideband Signals*, Acoustical Imaging, Vol. 19, Plenum Press Springer, 915–919.
17. NEILSON R.O. (1991), *Sonar Signal Processing*, Artech House.
18. PACE P.E. (2009), *Detecting and Classifying Low Probability of Intercept Radar*, 2 ed., Artech House.
19. PAPOULIS A. (2002), *Probability, Random Variables and Stochastic Processes*, (Fourth Edition), McGraw-Hill.
20. ROSHEN J., TESSAMMA T., UNNIKRISHNAN A. (2009a), *Fractional Fourier Transform Based Chirp Detector Versus Some Conventional Detectors*, International Symposium on Ocean Electronics (SYMPOL), Cochin India, 56–65.
21. ROSHEN J., UNNIKRISHNAN A., TESSAMMA T. (2009b), *Applications of Fractional Fourier Transform in Sonar Signal Processing*, IETE Journal of Research, **55**, 1, 16–27.
22. SALAMON R. (2006), *Sonar Systems* [in Polish], Gdańskie Towarzystwo Naukowe, Gdańsk.
23. SALAMON R., MARSZAL J., SCHMIDT J., RUDNICKI M. (2011), *Silent Sonar with Matched Filtration*. Hydroacoustics, Vol. **14**, Gdańsk, 199–208.
24. SALAMON R., MARSZAL J. (2013), *Estimating Intercept Range of Silent Sonar*, [in:] Hydroacoustics of Shallow Water, E. Kozaczka, G. Grelowska [Eds.], Polish Academy of Sciences Institute of Fundamental Technological Research Warszawa, 139–158.
25. SKOLNIK M. (2008), *Radar Handbook*, (Third Edition), McGraw-Hill Professional.
26. SREEDAVY E.N., PRADEEPA R., FELIX V.P. (2009), *A Novel Algorithm for Intercept Sonar Signal Detector*, International Symposium on Ocean Electronics (SYM-POL), Cochin India, 3–8.
27. THALES-SAFARE (2012), *VELOX-M8 Passive Intercept Sonar*, <http://www.thales-safare.com/pdf/VELOX-M8%20Oct2012L.pdf>.
28. URICK R.J. (1996), *Principles of Underwater Sound*, (Third Edition), Peninsula Pub.
29. WAITE A.D. (2002), *Sonar for practising engineers*, (Third Edition), John Wiley&Sons.
30. WARD M.K., STEVENSON M. (2000), *Sonar Signal Detection and Classification using Artificial Neural Networks*, Canadian Conference on Electrical and Computer Engineering, Vol. 2, Halifax, 717–721.
31. WILLETT P., REINERT J., LYNCH R. (2004), *LPI Waveforms for Active Sonar?*, IEEE Aerospace Conference Proceedings, 2237–2248.